WELDING RESEARCH

SUPPLEMENT TO THE *WELDING JOURNAL*, JANUARY 2000
Sponsored by the American Welding Society and the Welding Research Council

A Method for Studying Weld Fusion Boundary Microstructure Evolution in Aluminum Alloys

Nondendritic equiaxed grain microstructures were simulated in Li-bearing Alloy 2195

BY A. KOSTRIVAS AND J. C. LIPPOLD

ABSTRACT. Aluminum alloys may exhibit a variety of microstructures within the fusion zone adjacent to the fusion boundary. Under conventional weld solidification conditions, epitaxial nucleation occurs off grains in the heat-affected zone (HAZ) and solidification proceeds along preferred growth directions. In some aluminum alloys, such as those containing Li and Zr, a nondendritic equiaxed grain zone (EQZ) has been observed along the fusion boundary that does not nucleate epitaxially from the HAZ substrate. The EQZ has been the subject of considerable study because of its susceptibility to cracking during initial fabrication and repair. The motivation of this investigation was to develop a technique that would allow the nature and evolution of the fusion boundary to be studied under controlled thermal conditions.

A melting technique was developed to simulate the fusion boundary of aluminum alloys using the Gleeble® thermal simulator. Using a steel sleeve to contain the aluminum, samples were heated to incremental temperatures above the solidus temperature of a number of alloys. In Alloy 2195, a 4Cu-1Li alloy, an EQZ could be formed by heating in the temperature range approximately from 630–640°C. At temperatures above 640°C, solidification occurred by the normal epitaxial nucleation and growth mechanism. Fusion boundary behavior was also studied in Alloys 5454-H34, 6061-T6 and 2219-T8. Nucleation in these alloys was observed to be epitaxial. Details of the technique and its effectiveness for performing controlled melting experiments at incremental temperatures above the solidus are described.

A. KOSTRIVAS and J. C. LIPPOLD are with Welding and Joining Metallurgy Group; Department of Industrial, Welding and Systems Engineering; The Ohio State University; Columbus, Ohio.

Introduction

Weldability of aluminum alloys is a major issue during weld fabrication and repair and, in many alloy systems, is significantly influenced by the nature of structures developed along the weld fusion boundary (Ref. 1). For example, a new generation of Li-bearing aluminum alloys, which are used in high-performance lightweight aerospace structures (such as the main tank of the space shuttle), have been plagued with fusion boundary cracking problems during fabrication and repair. This cracking has been associated with an unusual equiaxed grain microstructure that forms in the fusion zone adjacent to the fusion boundary and is not predicted based on the conventional understanding of weld solidification. Other aluminum alloy systems with only slightly different compositions do not exhibit this microstructure and are observed to undergo "normal" solidification behavior and are free from fusion boundary cracking. There are few experimental methods currently available that allow the mechanism of fusion boundary microstructure evolution to be simulated or that predict when "good" and "bad" microstructures will form.

Solidification structure along the weld fusion boundary seems to play an important role in cracking susceptibility in some aluminum alloys. Li-bearing aluminum alloys may exhibit cracks along an equiaxed grain zone (EQZ) (Refs.1, 4), formed next to the weld fusion boundary. Other aluminum alloys do not show formation of such a structure and are less prone to crack formation in this region. In

KEY WORDS

Aluminum Alloys
Heat-Affected Zone
HAZ
Nucleation
Hot Cracking
Li-Bearing Alloys
Thermal Simulation
Gleeble®

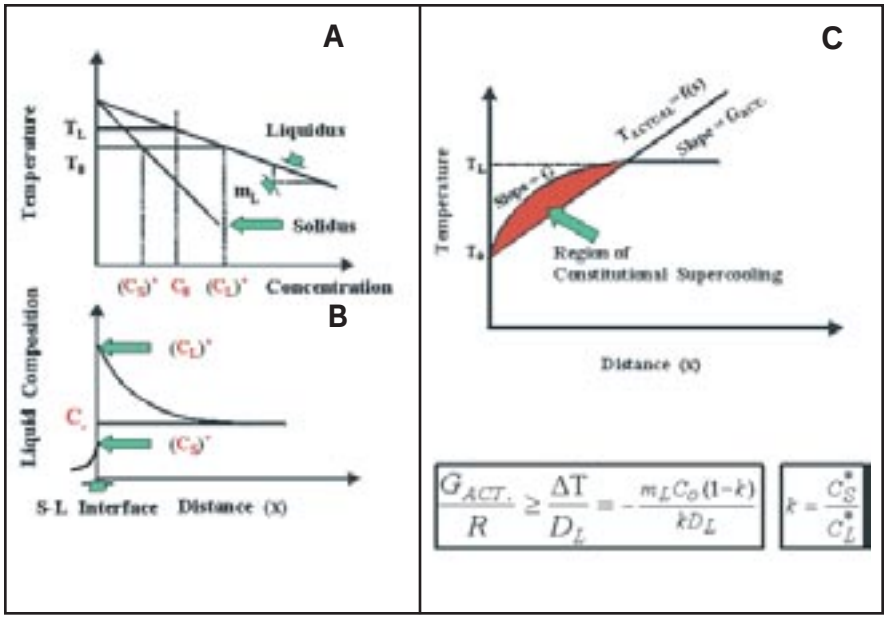

Fig. 1 — Constitutional supercooling during alloy solidification. A — Phase diagram; B — solute-enriched layer; C — unstable (supercooled) interface. The criterion for morphological stability for a moving solidification front with velocity R is also shown (Refs. 11–13).

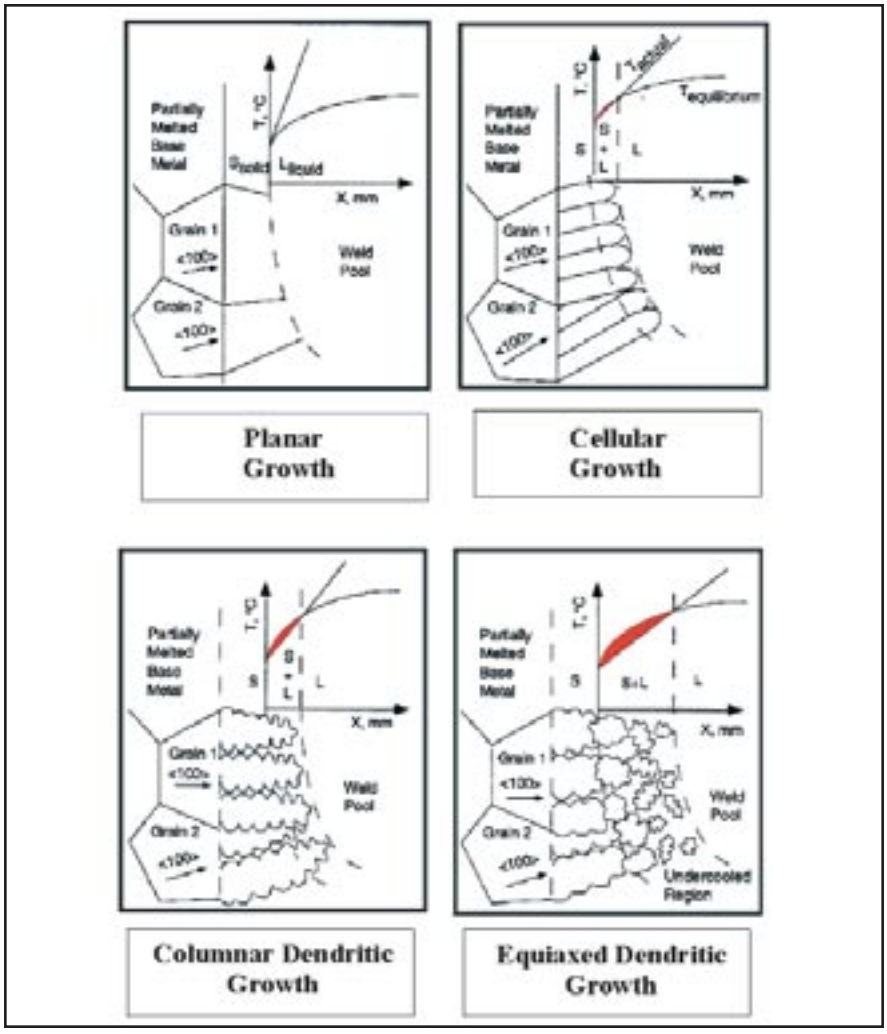

Fig. 2 — Mode of solidification vs. amount of constitutional supercooling (Ref. 12).

general, equiaxed grains in aluminum alloy welds are thought to be beneficial with respect to cracking (Refs. 5–10), so this behavior is surprising.

The constitutional supercooling (Ref. 11) theory has been developed to explain morphological stability along an advancing solidification front. For a binary alloy system and a given composition C_0, a variation in liquidus temperature is developed ahead of the advancing solid-liquid interface, attributable to solute buildup (partition coefficient $k < 1$), as shown in Fig. 1. If the actual thermal gradient $G_{act.}$ at the solid-liquid interface is greater than that for the predicted liquidus temperatures (G), then a planar front is maintained. When $G_{act.} < G$, then the solidification process results in instability of the planar front and interfacial breakdown occurs. This condition is known as constitutional supercooling since the supercooling arises from a change in composition immediately ahead of the advancing solid-liquid interface. The amount of supercooling dictates the mode of solidification (Fig. 2) and the associated morphology of the solidified microstructure, *i.e.,* cellular, dendritic or equiaxed dendritic subgrains.

During welding, the aforementioned subgrains nucleate directly from randomly oriented grains in the HAZ, which form the substrate at the fusion boundary. The driving force required for nucleation is low since the thermodynamic barrier for solidification is almost eliminated and only growth of new grains occurs. Each of these subgrains solidifies along a crystallographic direction dictated by the orientation of the parent grain in the HAZ, described as epitaxial growth. Subgrains with their solidification growth direction parallel to that of the maximum temperature gradient grow faster than others less favorably oriented, and this results in formation of solidification grain boundaries at regions where these subgrains impinge (competitive growth).

A number of models for weld solidification have been developed (Refs. 14–16), but few experimental techniques to verify these models have evolved. Direct observation of weld solidification has proven difficult due to both the scale of the solidification subgrains (on the order of microns) and the high temperatures associated with the solidification process.

Simulation of metallurgical and welding processes has been proven a practical and cost-effective means for studying new materials and optimizing both process- and material-related parameters. The Gleeble thermo-mechanical simulator has been extensively used to study metallurgical phenomena related

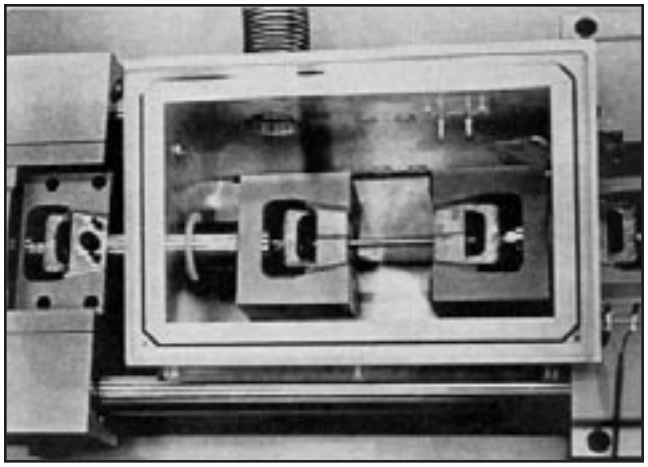

Fig. 3 — View of the atmosphere tank and gripping assembly of the Gleeble® 1500.

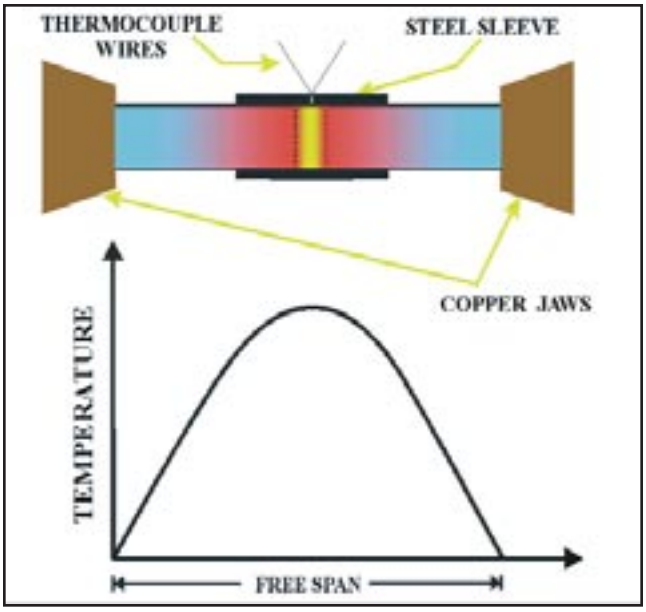

Fig. 4 — Schematic showing sample configuration for Gleeble® thermal simulation and the associated axial thermal gradient.

to the heat-affected zone (HAZ), *e.g.*, hot ductility behavior, precipitation kinetics, stress-relief cracking, strain-age cracking, constitutional liquation, etc.

Simulation of metallurgical behavior in the fusion zone has proven to be much more of a challenge using the Gleeble due to problems associated with containing the molten metal. This can be a particular issue with aluminum because relatively high currents are needed to heat the samples and maintaining thermocouple contact with the molten metal can be difficult (Refs. 2, 3). These problems can literally result in the sample "exploding" due to loss of containment or thermocouple contact. In this investigation, the use of a simple steel sleeve fitted around the aluminum sample was found to effectively contain the molten aluminum while allowing the temperature of the molten region to be monitored.

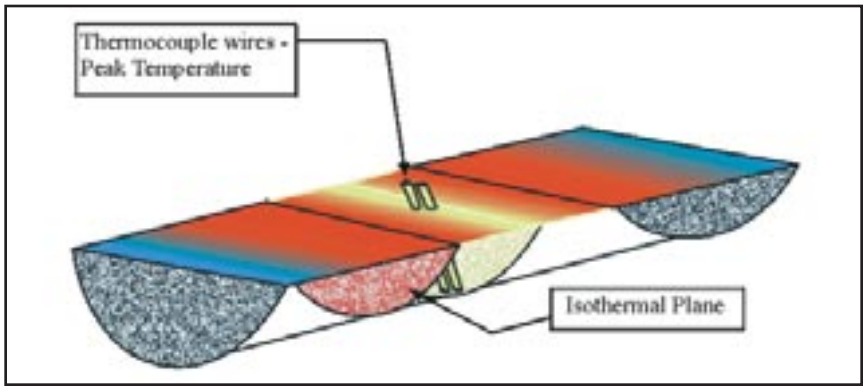

Fig. 5 — An axial slice of cylindrical sample heated by the Gleeble®. Thermocouple location and isothermal planes are shown.

Experimental Approach

Materials

Commercially available aluminum Alloys 2219-T8, 6061-T6 and 5454-H34 were investigated along with the Al-Cu-Li alloy 2195-T8. Cylindrical specimens used in this study were 102 mm (4 in.) long and 5 mm (0.196 in.) in diameter. The composition of these alloys is listed in Table 1.

Equipment Characteristics

The Gleeble® 1500 thermo-mechanical simulator was used to perform the controlled melting experiments. The gripping *(i.e.,* jaw) assembly within a vacuum, or atmosphere, tank is shown in Fig. 3. The Gleeble allows the simulation of complex thermal and mechanical cycles in small samples, while allowing continuous thermal monitoring and feedback control.

The specimen is held between two sets of water-cooled grips and heated by its own resistance (I^2R heating) by the passage of 60-Hz alternating electric current. An axial thermal gradient is created since the heat generated is being continuously extracted by conduction through the massive copper grips — Figs. 3 and 4.

Despite the small amount of heat radiation and/or convection from the specimen surface to the surrounding atmosphere, the radial temperature gradient is nearly zero due to uniform heating of the specimen. In addition, metallographic evaluation of isothermal sections revealed no change in microstructure in the melt zone adjacent to the steel con-

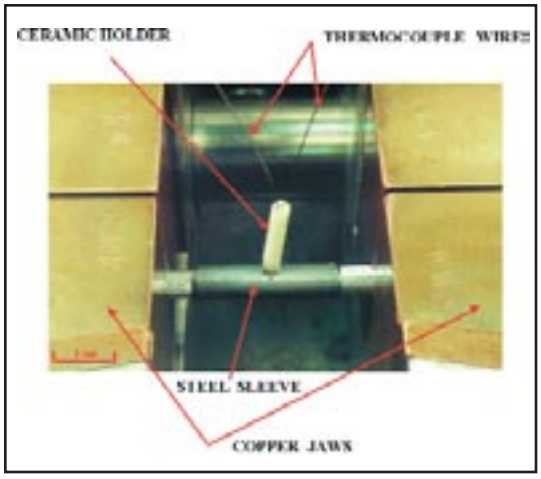

Fig. 6 — Experimental configuration for melting aluminum samples on the Gleeble®.

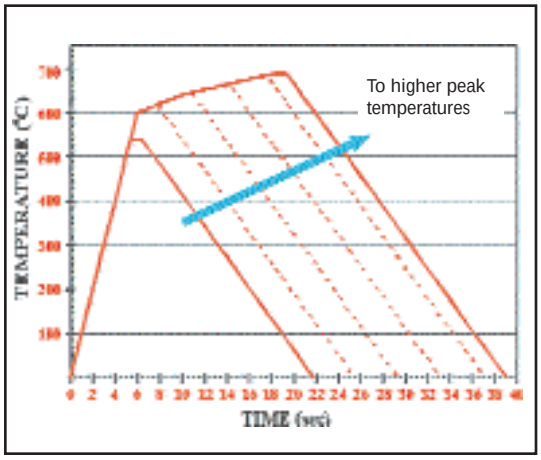

Fig. 7 — Typical thermal cycles applied (programmed) during controlled melting of aluminum samples.

tainment sleeve. Based on the small sleeve size (6.35 mm O.D.) and wall thickness (1.2 mm), it is assumed the sleeve reaches melt zone temperature. As a result, planes perpendicular to specimen axis are isothermal — Fig. 5. Temperature monitoring is achieved continuously via a thermocouple attached midspan on the specimen corresponding to the isothermal plane of maximum temperature. The output of the thermocouple is compared with the instantaneous value of the programmed temperature. The polarity and the magnitude of the error signal are used to determine the amount of the current flowing through the specimen, *viz.*, the specimen heating and cooling rates. The thermal profile generated by a given peak temperature, jaw separation, specimen size, geometry and material property is determined by a complex interrelation between the conduction, convection and radiation mechanisms in establishing a thermal balance.

Nil Strength Temperature Measurement

Initially, the nil strength temperature (NST) was determined for each alloy. The NST provides a good estimate of the fusion boundary temperature and was the starting point used for subsequent fusion boundary simulations. The test was performed by heating three samples of each alloy at a rate of 150°C/s under a small tensile load (approximately 10 lb). Heating continued until specimens failed. The temperature at failure was recorded as the NST.

Controlled Melting Experiments

Controlled melting samples were contained within a steel sleeve 2.54 cm (1 in.) long during heating in order to hold the molten aluminum in place. Other sleeve dimensions are given in the previous section. Clearance between the 5-mm-diameter sample and I.D. of the sleeve was approximately 0.1 mm (0.004 in.). A small hole 3 mm (0.12 in.) deep by 0.5 mm (0.02 in.) in diameter was drilled midspan in the aluminum specimens and a chromel-alumel thermocouple (0.25 mm diameter) was inserted through a hole machined in the steel tube. Thermocouple wires were mechanically attached to the specimen by mashing aluminum material around them. A ceramic dual-hole tube was slid around the thermocouple wires for even better stability and electrical insulation — Fig. 6.

The specimen assembly, located in the atmosphere chamber, was tightly secured in the water-cooled copper jaws — Fig. 6. Prior to testing, the chamber was evacuated and backpurged with argon to prevent specimens from oxidizing. After repeating the evacuation and argon purging procedure twice, melting simulation tests were performed in the protective atmosphere at nearly atmospheric pressure. Argon was flowing continuously during the test at minimal rate as a means to prevent air from entering into the chamber.

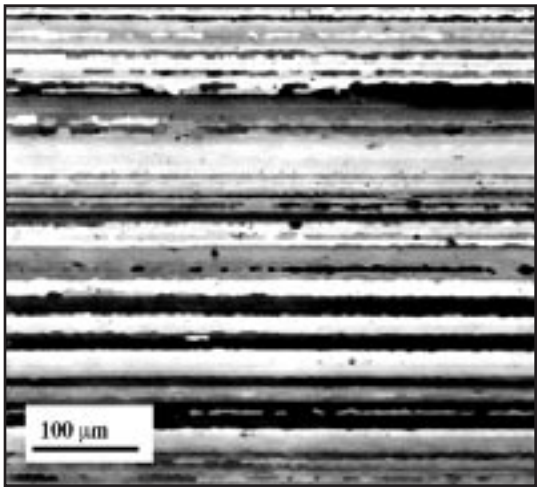

Fig. 8 — Alloy 2195-T8 base metal microstructure.

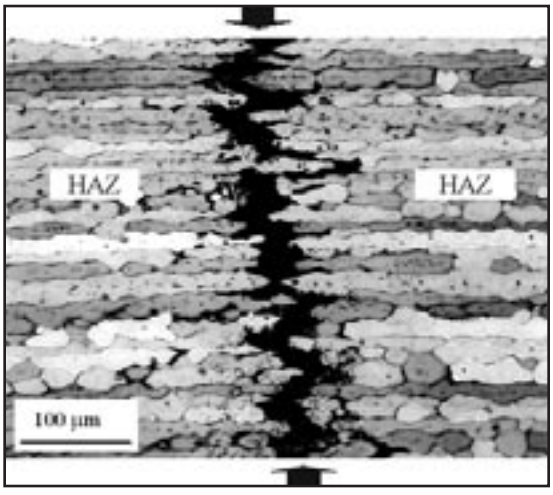

Fig. 9 — Weld fusion zone simulation of Alloy 2195-T8. Microstructure corresponds to specimen heated to 625°C: cooling rate = 60°C/s. Arrows highlight location of solidification crack.

Samples were heated to NST at a rate of 100°C/s. Above NST, heating to peak temperature was conducted at a rate of 7 to 1°C/s to control the melt zone. Specimens were held at peak temperature for 1 s and were control cooled at a programmed rate of 100°C/s, while the melt zone temperature was continuously monitored using the control thermocouple. Some deviations in the actual cooling rate from the program cooling rate were observed and were mainly attributable to release of latent heat from the melt. Tests were performed at temperature increments of approximately 10°C above NST — Figs. 4 and 7. It is possible to program a variety of different heating and cooling rates for each specimen configuration. However, the free span, *i.e.,* the distance between the surfaces of the two copper jaw sets (Fig. 4), remained constant at 3 cm (1.2 in.).

Metallurgical Evaluation

Following the melting simulation, specimens were sectioned axially, mounted, polished and etched with Barker's reagent for metallographic examination using polarized light. Polished sections were examined using an optical metallograph at magnifications up to 400X. Microhardness traverses were performed across the simulated fusion boundary using a Vickers indenter with a 100-g load.

Results and Discussion

Nil Strength Temperature

The NST was determined for each aluminum alloy and the values measured are presented in Table 2. The values reported here may be slightly lower than the actual NST since a small amount of force was applied on specimens during heating. NST is close to the "effective" solidus of the material, since considerable liquid is normally present in the microstructure. However, some of the values measured are below the nominal bulk solidus temperature reported in Table 2. Metallographic studies of aluminum alloys (Refs. 9, 17, 18) and in other systems (Ref. 19) suggest the NST closely approximates the temperatures at the fusion boundary in an actual fusion weld. These temperatures were used as the starting point for the controlled melting experiments.

Fusion Zone Simulation

Operational Procedure

Melting aluminum alloys on the Gleeble has been accomplished in the past using various techniques but presents considerable experimental challenges (Refs. 2, 3). Previous work using quartz containment tubes with an axial slot machined has proven troublesome since the tubes often cracked during testing. The use of steel tubes in this methodology avoids that problem and provides better containment if the relative specimen and tube sizes are properly controlled. Since steel has a much higher melting temperature than aluminum, there is no degradation of the sleeve material and no metallurgical interaction has been observed between the molten aluminum and steel. Another advantage is that aluminum has a higher coefficient of thermal expansion than steel over the temperature range from room temperature to 600°C, allowing the aluminum to expand into the sleeve and provide a tight seal at the ends.

Despite these advantages, some problems attributable to melt zone instability were encountered. Initially, it was difficult to contain the molten aluminum in the steel tube, and some "leaking" occurred through the small hole on the sleeve used for thermocou-

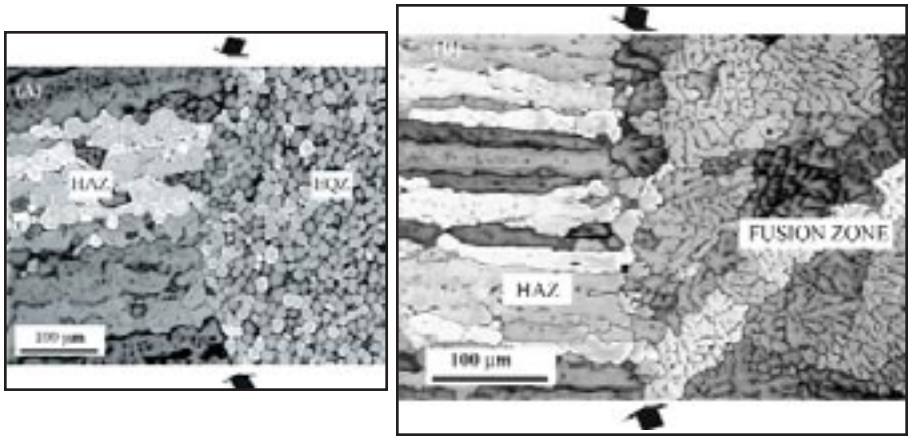

Fig. 10 — Simulated fusion boundary region in Alloy 2195-T8. Arrows indicate location of fusion boundary. A — 630°C, cooling rate = 65°C/s; B — 660°C, cooling rate = 30°C/s.

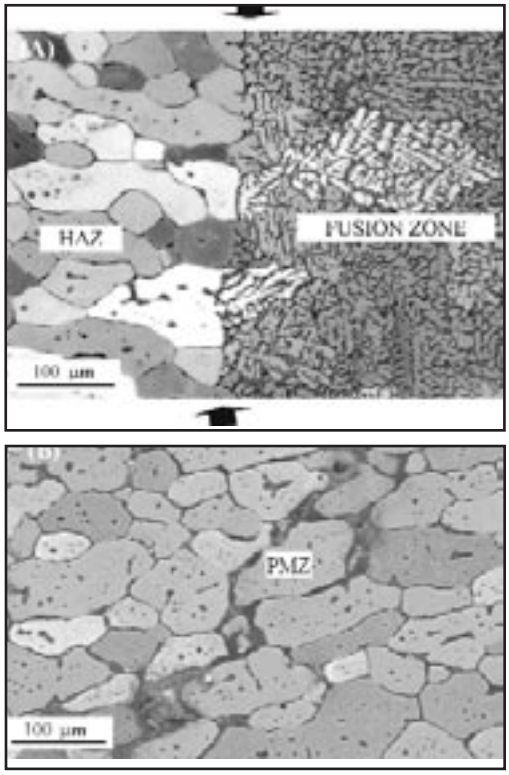

Fig. 11 — Simulated fusion boundary region in Alloy 6061-T6. Arrows indicate location of fusion boundary. A — 645°C, cooling rate = 46°C/s; B — 620°C, cooling rate = 90°C/s.

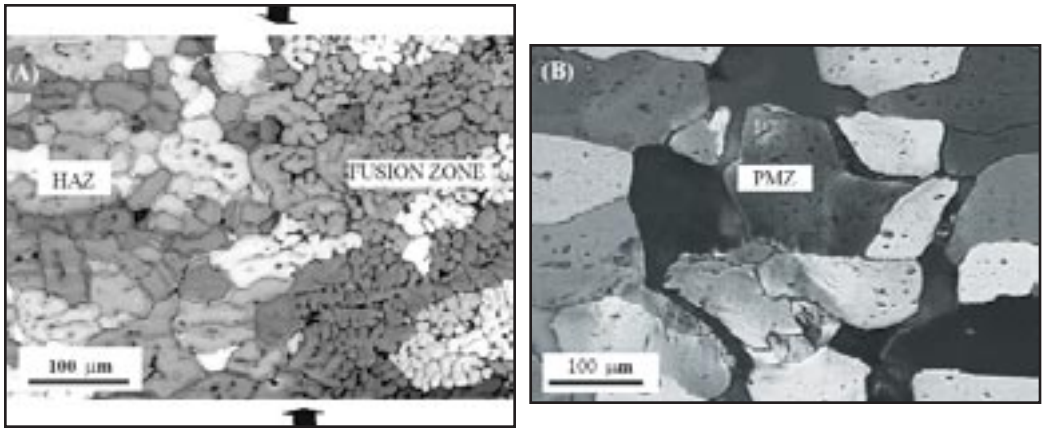

Fig. 12 — Simulated fusion boundary region in Alloy 2219-T8. Arrows indicate location of fusion boundary. A — 655°C, cooling rate = 30°C/s; B — 587°C, cooling rate = 85°C/s.

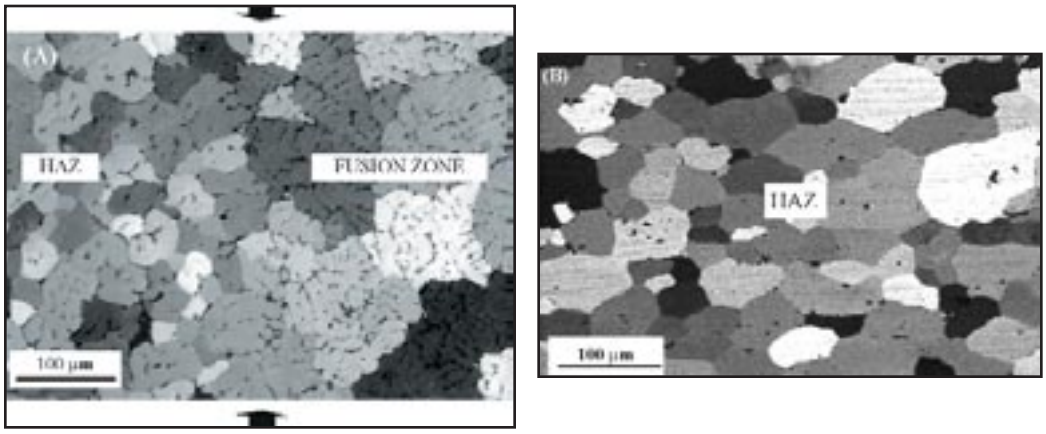

Fig. 13 — Simulated fusion boundary region in Alloy 5454-H34. Arrows indicate location of fusion boundary. A — 623°C, cooling rate = 87°C/s; B — 610°C, cooling rate = 87°C/s.

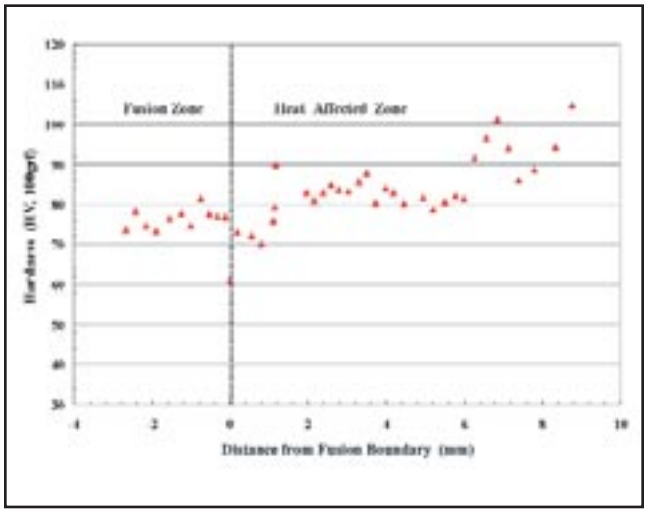

Fig. 14 — Hardness traverse across the fusion boundary for Alloy 2219-T8. Specimen was heated to a peak temperature of 640°C.

ple access. This problem was exacerbated at higher heating rates and prolonged times at peak temperature. Experiments conducted in vacuum aggravated the melt zone instability, possibly due to degassing effects.

Aluminum has low resistance (high conductivity), and thus large currents are required to achieve melting. This, in turn, results in strong electromagnetic pinch forces. It has been proposed (Ref. 2) that as soon as the molten zone is formed, the pinch forces produce necking of the molten region. Once the necking takes place, the reduced cross-sectional area promotes higher current density and, in turn, necking is augmented. In addition, the thermocouple response is slower when suspended in the molten zone than when the thermocouple wires are welded directly to the specimen (Ref. 3). Hence, a local instantaneous overheating and melt zone instability leads to removal of a significant mass of molten aluminum out of the crucible. It was found that using slower heating rates (Fig. 7) at the temperature range beyond NST, along with reduced dwell time at peak temperature, minimized that effect and resulted in a less vigorous melting process. Reducing the number of heat cycles after the specimen temperature exceeds NST also helps stabilize the aluminum melting process by reducing the liquid stirring. At temperatures above the NST, the liquid state becomes dominant within a narrow temperature range, thus enabling a lower amount of current to flow to keep temperature constant. By deleting one, two or three heating cycles, each operating cycle is still at power line frequency. Hence, the approximate I_{RMS} value can be decreased by 29, 43 and 50%, respectively, in each case. This feature allows better control over the temperature of the melt since low heating frequency results in both smaller heating current and longer time over which a weak magnetic field occurs, which finally helps prevent molten metal from overheating and being expelled from the steel crucible. The outcome is a robust melting technique accompanied by a high level of success.

Characterization Results

Optical microscopy has revealed that melting/solidification tests on the Gleeble can reproduce the various regions surrounding the fusion boundary in Alloy 2195.

In all alloys, except 2195, the melt zone microstructure was uniformly dendritic. The wrought base metal mi-

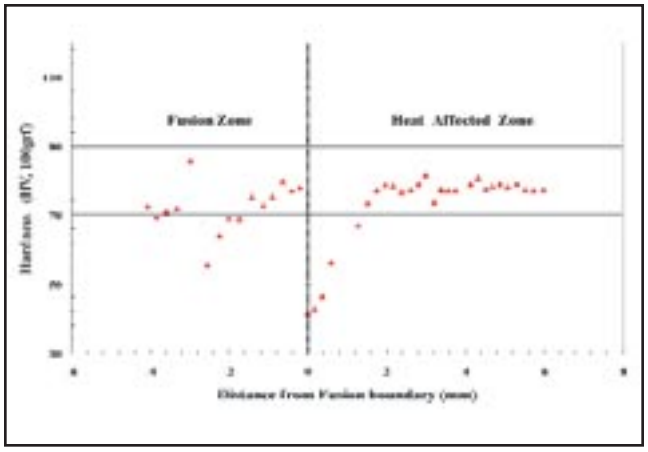

Fig. 15 — Hardness traverse across the fusion boundary for Alloy 6061-T6. Specimen was heated to a peak temperature of 645°C.

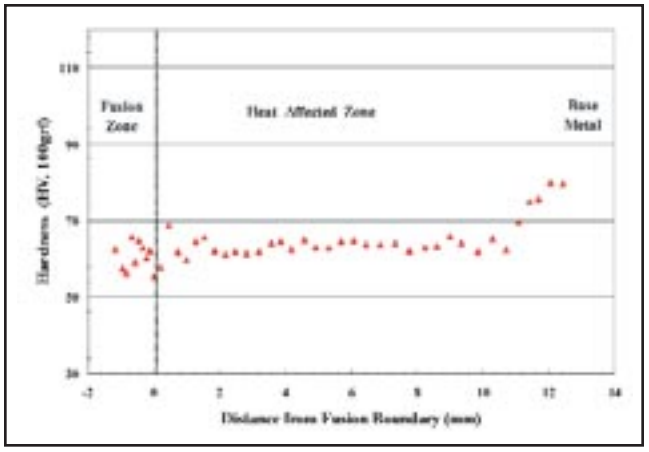

Fig. 16 — Hardness traverse across the fusion boundary for Alloy 5454-H34. Specimen was heated to a peak temperature of 623°C.

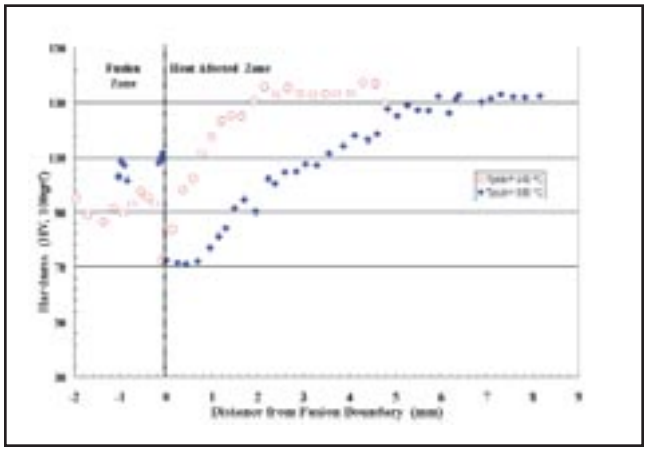

Fig. 17 — Hardness traverse across the fusion boundary for Alloy 2195-T8. Specimens were heated at peak temperatures of 630 and 640°C.

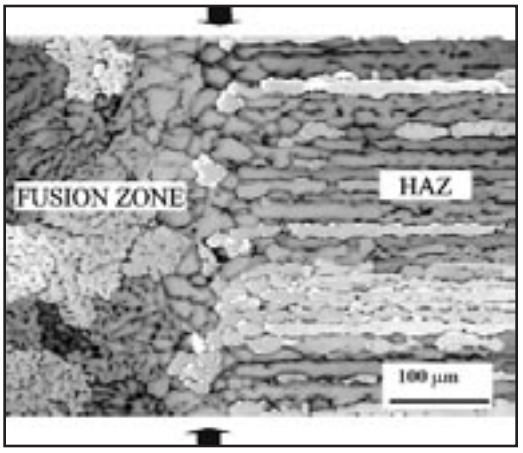

Fig. 18 — Simulated fusion boundary region in Alloy 2195-T8. Arrows indicate location of fusion boundary. Specimen heated to 640°C peak temperature, cooling rate = 40°C/s.

crostructure of Alloy 2195 is shown in Fig. 8. In samples heated to the NST (~625°C), gross melting is not observed and the microstructure is similar to the partially melted zone (PMZ) observed adjacent to the fusion boundary. This region, shown in Fig. 9, exhibited a crack due to the shrinkage strains within the sample during cooling. When heated into the temperature from approximately 630 to 640°C, nondendritic equiaxed growth occurs, as shown in Fig. 10A. When heated above 640°C, standard epitaxial nucleation and growth occurs off the substrate and dendritic microstructures are observed — Fig. 10B. Some equiaxed grains may be observed at the solid-liquid interface.

When 6061 is heated above its NST (~591°C), only epitaxial dendritic growth occurs — Fig. 11. There appears to be no tendency for nondendritic EQZ formation in this alloy. Similar behavior was observed for Alloys 2219 and 5454, irrespective of the peak temperature applied — Figs. 12 and 13.

Hardness traverses made from the base metal across the fusion boundary for Alloys 2219-T8 and 6061-T6 show typical HAZ degradation (softening) due to precipitation dissolution and/or precipitate coarsening — Figs. 14 and 15. The extensive softening observed in the HAZ of Alloy 5454-H34 can be attributed to recovery, recrystallization and grain growth — Fig. 16.

Alloy 2195-T8 also exhibited a softening reaction in the HAZ due to reversion and overaging. However, a sharp increase in hardness was observed (Fig. 17) within the EQZ. This hardness increase disappeared in samples heated at higher peak temperatures having a dendritic structure upon solidification — Figs. 17 and 18. This is consistent with hardness traverses reported across the fusion boundary of actual welds in this alloy (Refs. 21, 22). It is proposed that the higher hardness in the EQZ is related to both the finer grain size and the higher proportion of eutectic constituents relative to the epitaxial, dendritic structure.

Transmission electron microscopy (TEM) investigation of the 2195 samples is under way to support the theory (Refs. 23, 24) that Zr-rich particles act as nucleants for the equiaxed grains in the narrow temperature regime above solidus. Based on the controlled melting experiments, it appears that above 640°C, in

the bulk of melt zone, these particles dissolve and are unavailable as nucleants, allowing epitaxial nucleation to proceed. Altering the base metal substrate has also been shown to influence EQZ formation. For example, shifting from wrought to a cast substrate minimizes or eliminates EQZ formation (Ref. 4) in Alloy 2195. It is expected these structures will consistently be reproduced by thermal simulation, and subsequent TEM analysis will help to verify the absence of any nucleating particles in the resulting cast structures. Results to date have clearly eliminated the recrystallization and grain growth mechanism for EQZ that had been proposed by other investigators (Ref. 25).

This investigation has demonstrated that controlled melting of aluminum alloys can be accomplished routinely and that this method is very useful for studying fusion boundary behavior. Using controlled melting experiments at temperatures 10 to 50°C above the NST, a model for fusion boundary microstructure evolution based on composition, substrate microstructure and thermal conditions will be developed in the context of the aluminum alloy systems evaluated.

Conclusions

1) A melting technique has been developed that allows fusion boundary microstructure evolution in aluminum alloys to be studied using the Gleeble® thermal simulator.

2) A steel tube acting as crucible in conjunction with special heating procedures at temperatures slightly above the nil-strength temperature resulted in a controlled melting process.

3) The effect of thermal conditions on the equiaxed grain zone (EQZ) in the Li-bearing Alloy 2195 has been identified. The EQZ was found to form in the temperature range from 630 to 640°C.

4) A sharp increase in hardness observed within the EQZ of Alloy 2195 is eliminated when it solidifies epitaxially and exhibits a dendritic structure.

5) The nature of fusion boundary microstructure evolution in alloys 6061, 5454 and 2219 is dictated primarily by epitaxial nucleation and growth.

Acknowledgments

Appreciation is expressed to the staff of Dynamic Systems, Inc., for their technical assistance. In addition, gratitude is due to Dr. G. M. Goodwin and Dr. H. W. Kerr for helpful discussions. Thanks are also extended to Dr. Stan David at Oak Ridge National Labs for providing the DTA results on Alloy 2195.

References

1. Kostrivas, A., and Lippold, J. C. Weldability of Li-bearing aluminum alloys: A review. To be published in *International Materials Reviews* 44(5).

2. Chen, C. C., and Baeslack III, W. A. 1988. Weld fusion zone simulation in aluminum alloy 2090. *The International Symposium of Physical Simulation of Welding, Hot Forming and Continuous Casting*, ed. J. A. Bowker. Ottawa, Canada, pp. IV55–IV64.

3. Batra, R., Wilber, G. A., Breit, H. F., and Childs, W. J. 1975. Programmed in situ melting, freezing, and tensile testing for laboratory study of high temperature properties of as-cast metals. *Journal of Testing and Evaluation* 3(1): 68–74.

4. Gutierrez, A. E., and Lippold, J. C. 1998. A proposed mechanism for equiaxed grain formation along the fusion boundary in aluminum-copper-lithium alloys. *Welding Journal* 77(3): 123-s to 132-s.

5. Dvornak, M. J., Frost, R. H., and Olson, D. L. 1989. The weldability and grain refinement of Al-2.2Li-2.7Cu. *Welding Journal* 68(8): 327-s to 335-s.

6. Lees, D. G., and Member, M. A. 1946. The hot-tearing tendencies of aluminum casting alloys. *Journal of Institute of Metals* 72: 343–364.

7. Eeghem, J., and Sy, A. De. 1965. A contribution to understanding the mechanism of hot tearing of cast steel. *Modern Castings* 48: 100–109.

8. Spencer, B., Mehrabian, R., and Flemings, M. C. 1972. Rheological behavior of Sn-15 pct Pb in crystallization range. *Metallurgical Transactions* 3: 1925–32.

9. Boyle, J. P., Mannas, D. A., and Walsh, D. W. 1992. The effects of grain size on hot cracking of welded 2014 aluminum alloy rolled ring forgings. *Fifth International Symposium on Physical Simulation*. Delft, Netherlands, pp. 165–173.

10. Nelson, T. W. 1993. Development of a circular patch test for assessing weld solidification cracking. Master's thesis, The Ohio State University, Columbus, Ohio.

11. Kurz, W., and Fisher, D. J. 1984. *Fundamentals of Solidification.* Aedermannsdorf, Switzerland, Trans Tech SA, pp. 51–92.

12. Kou, S. 1987. *Welding Metallurgy*. John Wiley & Son, New York, N.Y., p. 168.

13. Grong, O. 1994. *Metallurgical Modelling of Welding.* The Institute of Materials, London, U.K., p. 225.

14. Flemings, M. C. 1974. *Solidification Processing.* McGraw-Hill, Inc., New York, N.Y.

15. Kou, S., and Le, Y. 1986. Nucleation mechanisms and grain refining of weld metal. *Welding Journal* 65(12): 305-s to 313-s.

16. David, S. A., and Vitek, J. M. 1989. Correlation between solidification parameters and weld microstructures. *International Materials Reviews* 34(5): 213–245.

17. Balaguer, J. P., Walsh, D. W., and Nippes, E. F. 1989. Hot ductility response of Al-Mg and Al-Mg-Li alloys. *Welding Journal* 68(7): 253-s to 261-s.

18. Lippold, J. C., Lin, W., Baeslack III, W. A., Xia, D., and Szabo, A. 1994. Weld cracking susceptibility of aluminum-lithium alloys. *Aluminum-Lithium Alloys for Aerospace Applications Workshop*, NASA Conference Publication 3287, pp. 288–289.

19. Lin, W. 1991. A methodology of quantifying heat-affected zone liquation cracking susceptibility. Ph.D. dissertation, The Ohio State University, Columbus, Ohio.

20. *ASM Handbook*. 1998. Properties and selection of nonferrous alloys and special purpose materials. Vol. 2, pp. 79, 97, 103.

21. Martukanitz, R. P., Lysher, K. G., and Howell, P. R. 1994. Laser beam welding of aluminum-lithium structures, NASA Conference Publication 3287, pp. 237–244.

22. Baeslack III, W. A., and Hou, K. H. 1996. Characterization of the heat-affected zone in gas tungsten arc welded aluminum alloy 2195-T8. *Journal of Materials Science Letters,* 15: 239–244.

23. Lippold, J. C., and Lin, W. 1996. Weldability of commercial Al-Cu-Li alloys. *Fifth International Conference on Aluminum Alloys*. Eds., J. H. Driver, F. Durand, R. Fougeres, P. Guyot, P. Sainfort and M. Suery, Grenoble, France, Vols. 217–222, pp. 1685–1690.

24. Yunjia, H., Dalu, G., and Zhixiong, S. 1991. Solidification mode and cracking behavior of aluminum-lithium alloy welds. *Sixth International Aluminum-Lithium Conference*. Eds. M. Peters, and P. -J. Winkler, Garmisch-Partenkirchen, Germany, Vol. 2, pp. 1215–1220.

25. Shah, S. R., Wittig, J. E., and Hahn, G. T. 1993. Microstructural analysis of a high strength Al-Cu-Li (Weldalite™ 049) alloy weld. *International Trends in Welding Science and Technology*, pp. 281–285.